Electronic Supplementary Information

Efficient ambient ammonia synthesis by Lewis acid pair over cobalt single atom catalyst with suppressed proton reduction

Ngoc Quang Tran,[a≠] Xinghui Liu,[ab≠] Yunhee Cho,[ab] Thai Duy Le,[d] Lirong Zheng,[e] Jianmin Yu,[ab] Sara Ajmal,[ab] Xiaodong Shao,[ab] Jinsun Lee,[ab] Hyoyoung Lee*[abc]

[a.] *Center for Integrated Nanostructure Physics, Institute for Basic Science (IBS), Suwon 16419, Republic of Korea.*
[b.] *Department of Energy Science, Sungkyunkwan University, Suwon 16419, Republic of Korea.*
[c.] *Department of Chemistry, Sungkyunkwan University, Suwon 16419, Republic of Korea.*
[d.] *Department of Materials Science and Engineering, Ajou University, Suwon 16499, Republic of Korea.*
[e.] *Beijing Synchrotron Radiation Facility, Institute of High Energy Physics, Chinese Academy of Sciences, Beijing, China.*
≠ *The authors contributed equally*

Electrochemical measurements

Working electrode preparation. After treating in O_2 plasma at a pressure of 500 mTorr for 10 min, carbon fiber paper was used as the current collector. To prepare the catalyst ink, the mixing of 5 mg of catalyst, 10 µl of 5% Nafion 117 solution, 495 µl of ethanol, and 495 µl of deionized water were sonicated for 1 h to form a homogeneous ink. Subsequently, 60 µl of the catalyst ink was dropped onto both sites of a 1 x 1 cm^2 carbon fiber paper (mass loading of 0.3 mg/cm^2) and was naturally dried at room temperature for 12 h.

Electrochemical NRR measurements. All electrochemical measurements were carried out in a three-electrodes gas-tight two-compartment electrochemical cell in 0.01 M HCl electrolyte at ambient conditions using a VMP3 electrochemical workstation (Biologic Science Instruments, France). The reference electrode (Ag/AgCl in 3M KCl) and the working electrode were placed in the cathodic compartment. The Pt foil counter electrode was placed in the anodic compartment, separated by the Nafion membrane. Before use, the Nafion membrane was pretreated by successive boiling in a 5% H_2O_2 solution at 80 ºC for 1 h and deionized water for another 1 h at 80 ºC. All potentials in this study were converted to the RHE scale based on the Nernst equation. Before electrocatalytic experiments were performed, the 0.01 M HCl electrolyte at the cathodic compartment was purged by ultra-high purity N_2 (99.999%) gas for at least 1 h and was continuously fed (20 sccm) during the NRR test. After initial cyclic voltammetry sweeps, one-hour chronoamperograms at the different applied potential in N_2-saturated 0.01 M HCl were measured to evaluate the effects of various potentials on the NH_3 yield rate and Faraday efficiency.

Determination of the produced ammonia. The indophenol blue method was applied to determine a quantitative ammonia concentration in 0.01 M HCl electrolyte. Typically, 2 ml of the electrolyte

after electrolysis of nitrogen was added into a 2 ml of a 1 M NaOH solution containing 5 wt% salicylic acid and 5 wt% sodium citrate, and 1 ml of 0.05 M NaClO and 0.2 ml of 1 wt% $C_5FeN_6Na_2O$ were successively added into the above solution. After 3 h storage in the dark at room temperature, the mixture solutions were measured using a UV-vis absorption spectrophotometer. The concentration of indophenol blue was determined based on the absorbance peak at a wavelength of 655 nm. To estimate the concentration-absorbance calibration curves, the series of concentrations of standard NH_4^+ in 0.01 M HCl solutions were prepared.

Determination of the produced hydrazine. The Watt and Chrisp method was applied to determine the amount of hydrazine in the electrolyte. The colored solution was first prepared by mixing 1.497 g para-(dimethylamino) benzaldehyde, 7.5 ml concentrated HCl, and 75 ml ethanol. Then, 5 ml of the electrolyte after electrolysis of nitrogen was added into 5 ml of the coloring solution, following by stirring for 10 min. The absorbance of the resulting solution was measured at a wavelength of 460 nm. To estimate the concentration-absorbance calibration curves, a series of concentrations of standard hydrazine in 0.01 M HCl solutions were prepared.

$^{15}N_2$ isotopic labeling experiment. After one-hour electrolysis at -0.1 V *vs.* RHE using $^{15}N_2$ as a feed gas and argon as a protected gas, 8 ml of electrolyte was taken out and was concentrated to 2 ml. Then, 0.5 ml of the resulting solution was taken out, followed by the addition 20 µl of D_2O, which contains 1 w/w% of 3-(trimethylsilyl)-1-propanesulfonic acid sodium salt as an internal standard. The obtained $^{15}NH_4$ was quantitatively determined by 1H NMR spectroscopy.

The calculation method for Faraday efficiency and the yield rate

The Faraday efficiency (FE) and mass-normalized yield rate of the NH_3 product were calculated as follows:

$$FE = \frac{[N * F * c(NH_3) * V]}{Q}$$

$$Yield\ rate_{mass}(NH_3) = \frac{[17c(NH_3) * V]}{t * m}$$

N = 3: The number of electrons transferred for NH_3 product formation

F = 96485 C/mol: Faraday constant

c(NH_3): measured NH_3 concentration

V : volume of the HCl electrolyte

Q: total charge passed through the working electrode

t = 1 h: electrolysis time

m = 0.3 mg: the mass loading of the catalyst

The calculation method for Turnover Frequency (TOF) number

The TOF number for NH_3 was calculated as follow:

$$TOF = \frac{I_{NH3}\ \text{x}\ M_{Co}\ \text{x}\ 3600}{m\ \text{x}\ \omega\ \text{x}\ \delta\ \text{x}\ N\ \text{x}\ F}$$

I_{NH3}: Partial current for NH_3 production

N = 3: The number of electrons transferred for product formation

F = 96485 C mol^{-1}: Faraday constant

m: Catalyst mass in the electrode

M_{Co}: atomic mass of Co

δ: The molar ratio of surface atoms

ω: mass ratio of Co (%) in the catalyst

The molar ratio of surface atoms was calculated as follow:

By XRD in Supplementary Fig. 11 a, we confirmed that the as-prepared Co nanoparticle possesses a face-center cubic crystal structure with lattice constant (a) is 0.3521 nm. The radius of the Co sphere is denoted as R. The surface area of a single Co nanoparticle is $4\pi R^2$, whereas the area of each atom on the surface is $a^2/2$. Thus, the total number of atoms on the surface of a single Co nanoparticle is $8\pi R^2/a^2$. Secondly, the volume of a single Co nanoparticle is $4\pi R^3/3$. The volume of the unit cell for the face-center cubic crystal structure is a^3 with each unit cell containing 4 atoms. Therefore, the volume occupied by a single Co atom is $a^3/4$. So, the total number of atoms in a single Co nanoparticle is $16\pi R^3/3a^3$. Finally, the molar ratio of the surface atom for Co nanoparticle was calculated to be 3a/2R."

XAFS measurements. The X-ray absorption fine structure spectra of Co K-edge were collected at the 1W1B station in Beijing Synchrotron Radiation Facility (BSRF). The storage rings of BSRF were operated at 2.5 GeV with an average current of 250 mA. Using a Si (111) double-crystal monochromator, the data collection was carried out in transmission/fluorescence mode using an ionization chamber. All spectra were collected under ambient conditions.

XAFS Analysis and Results. The acquired EXAFS data were processed according to the standard procedures using the ATHENA module implemented in the IFEFFIT software packages. The k_3-weighted EXAFS spectra were obtained by subtracting the post-edge background from the overall absorption and then normalizing with respect to the edge-jump step. Subsequently, k^3-weighted $\chi(k)$ data of Co K-edge were Fourier transformed to real (R) space using Hanning windows (dk =

1.0 $Å^{-1}$) to separate the EXAFS contributions from different coordination shells. The least-squares curve parameter fitting was performed using the ARTEMIS module of IFEFFIT software packages to obtain the quantitative structural parameters around central atoms. The Fourier transforming of the k^3-weighted EXAFS data was performed in the range of k = 2.4-11.5 $Å^{-1}$ and R = 1-2.7 $Å^{-1}$ using a Hanning function window to get the radial distribution function. For Wavelet transform, we used the Morlet method by the own-writing program using the fitting parameter of kappa and sigma are 3 and 2.

Calculation method

The first principle density functional theory (DFT) calculations were conducted by means of the Vienna Ab initio Simulation Package (VASP) with the projector augmented wave (PAW) method.[1-4] The exchange-functional was treated using the generalized gradient approximation (GGA) with the Perdew-Burke-Ernzerhof (PBE) PBE+U_{eff} calculations.[5-7] The energy cutoff for the plane-wave basis expansion was set to 450 eV, and the force on each atom was set to be less than 0.03 eV/Å for the convergence criterion of geometry relaxation. A 5×5 supercell of graphene was employed with a 20 Å vacuum along the z-direction to avoid the interaction between periodic structures. The Brillouin zone integration was performed using 3×3×1 k-point sampling through all the computational process. The self-consistent calculations applied a convergence energy threshold of 10^{-4} eV. Due to the calculation deviation of the PBE functional in describing the partially filled d subshells of transition metal atoms, 4 eV as correlation energy (U) and 1 eV as the exchange energy (J) were used for Co atoms.[8] Besides, ab initio molecular dynamics (AIMD) simulations were performed at 300 K for 10 ps to evaluate the thermodynamic stability of CoN4@graphene.

The free energies of the N_2 reduction steps (NRR) were calculated by the equation: $\Delta G = \Delta E_{DFT} + \Delta E_{ZPE} - T\Delta S$, where ΔE_{DFT} is the DFT electronic energy difference of each step, ΔE_{ZPE} and Δ_S are the correction of zero-point energy and the variation of entropy, respectively, which are obtained by vibration analysis, and T is the temperature (T = 298 and 378 K).[9]

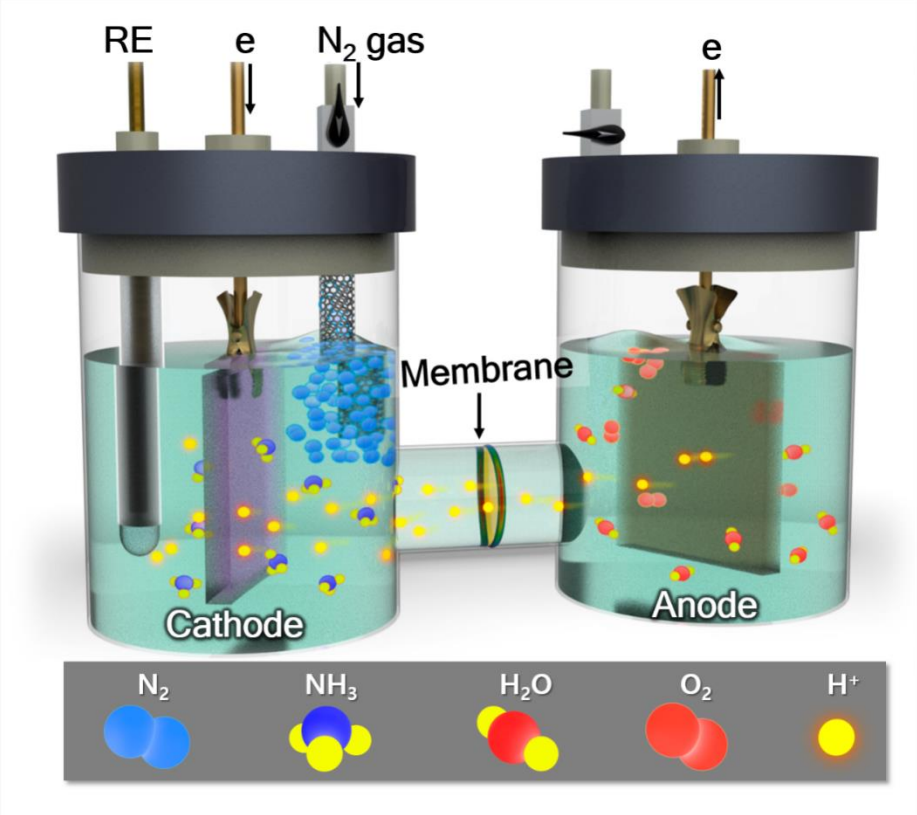

Supplementary schematic 1: *Schematic of electrochemical cell for NRR. The anode and cathode compartments are separated by a cation exchange membrane.*

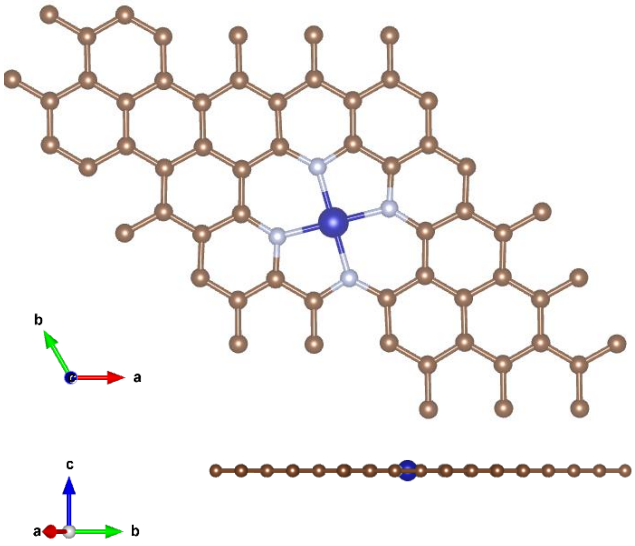

Supplementary Fig. 1 Top-view and side-view of structure prototype of CoN_4.

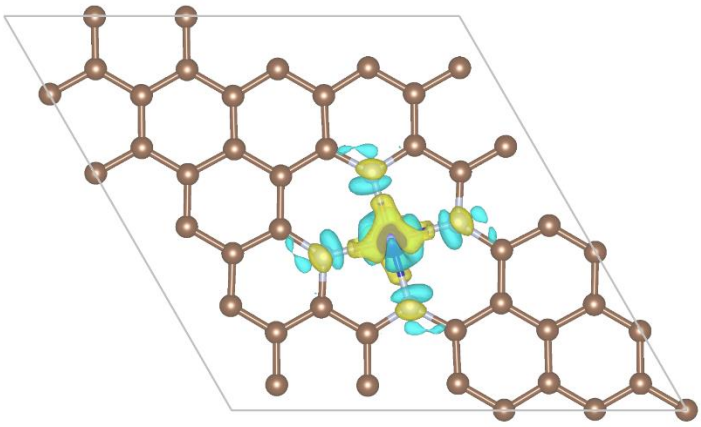

Supplementary Fig. 2 Top-view of different charge density map before $*N_2$ adsorption on CoN_4.

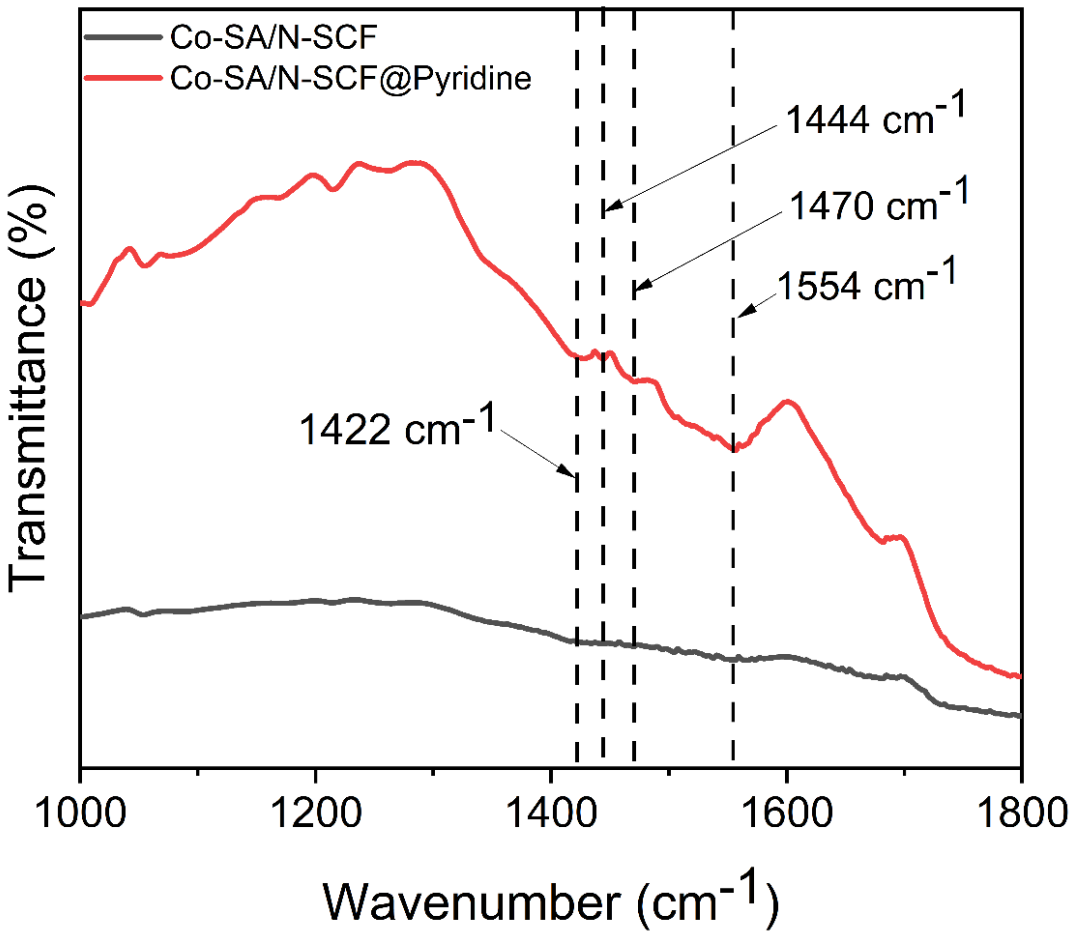

Supplementary Fig. 3. FT-IR spectra of Co-SA/N-SCF and Co-SA/N-SCF@Pyridine.

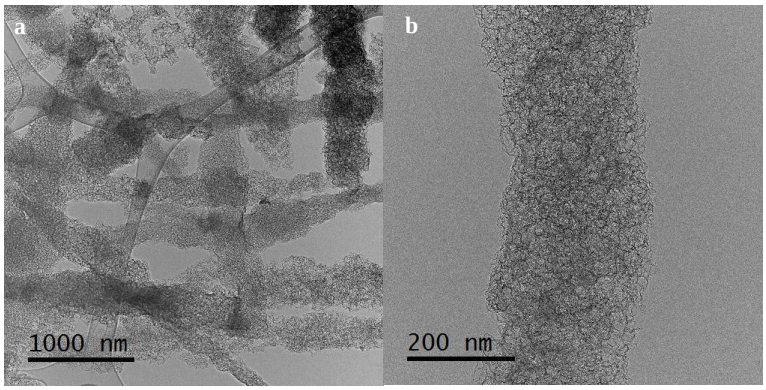

Supplementary Fig. 4 a HRTEM image with low and **b** high magnification of N-SCF.

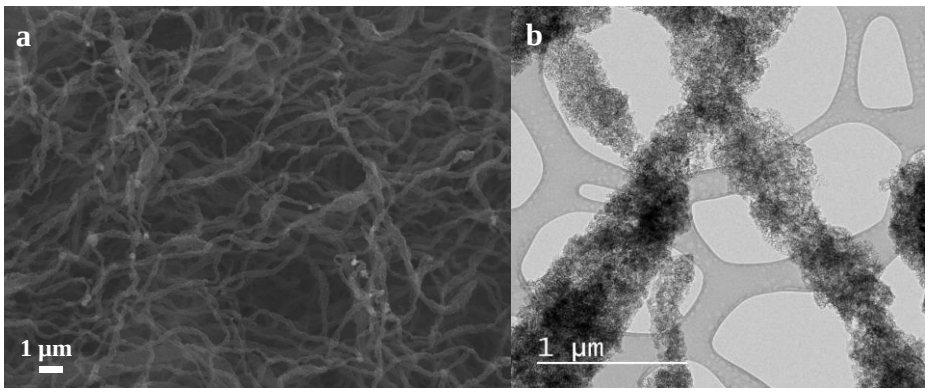

Supplementary Fig. 5 a FESEM and **b** HRTEM image of Co-SA/N-SCF catalyst.

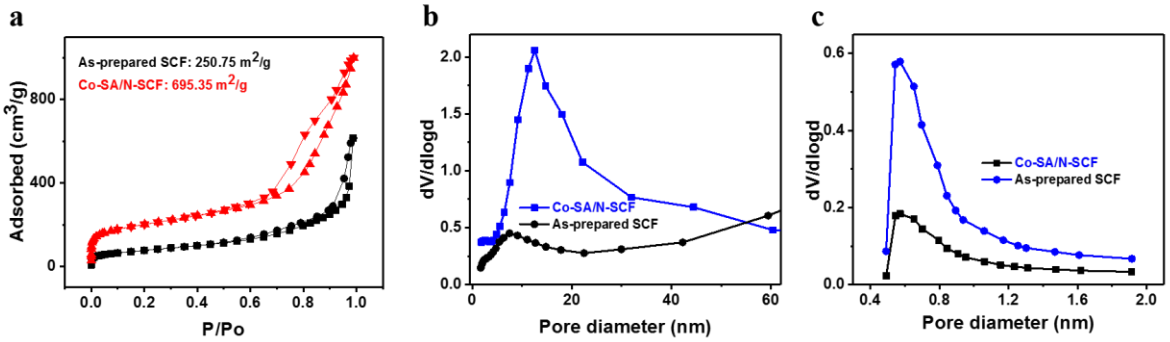

Supplementary Fig. 6 a BET surface area. **b** and **c** BJH pore size distribution of the Co-SA/N-SCF and pristine SCF.

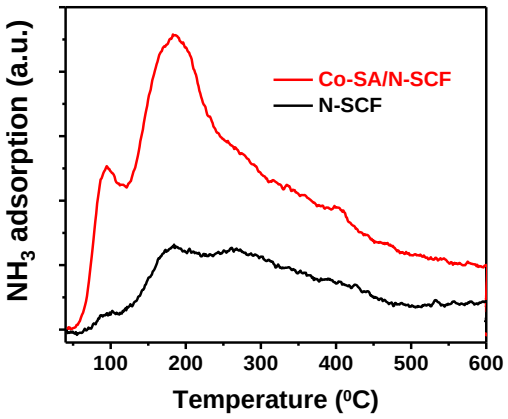

Supplementary Fig. 7 NH_3-TPD profiles of N-SCF and Co-SA/N-SCF catalysts.

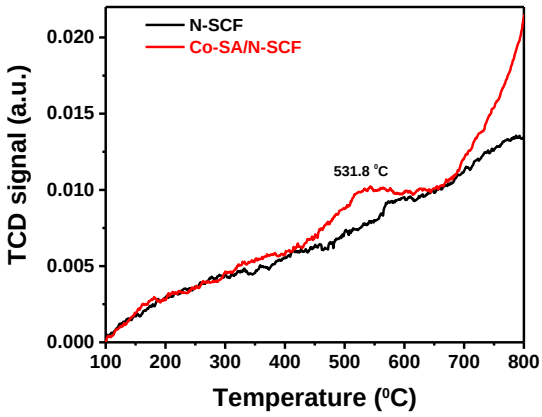

Supplementary Fig. 8 N_2 TPD patterns of N-SCF and Co-SA/N-SCF catalysts

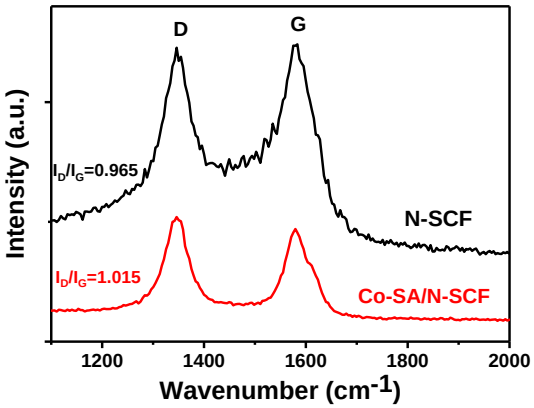

Supplementary Fig. 9 Raman spectra of Co-SA/N-SCF and N-SCF

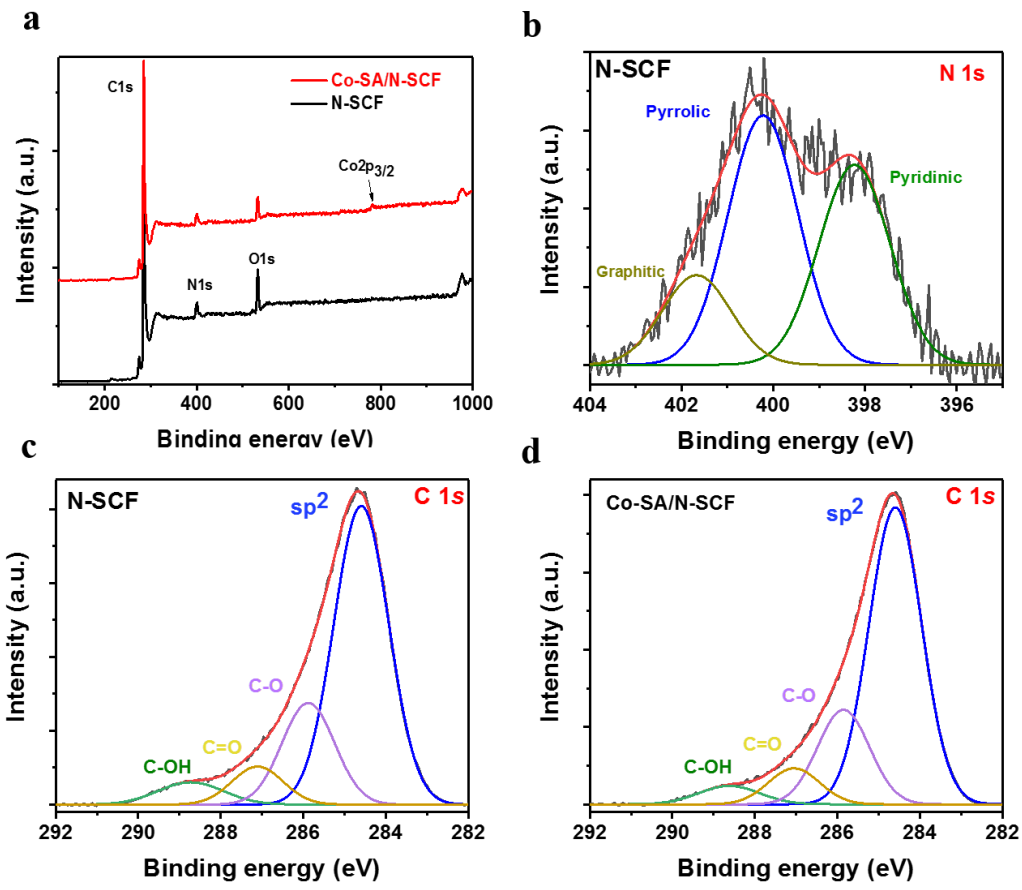

Supplementary Fig. 10 a XPS spectra for the survey scan of Co-SA/N-SCF and N-SCF. **b** High-resolution XPS N *1s* spectra of N-SCF. **c** High-resolution XPS C*1s* spectra of N-SCF. **d** High-resolution XPS C *1s* spectra of Co-SA/N-SCF.

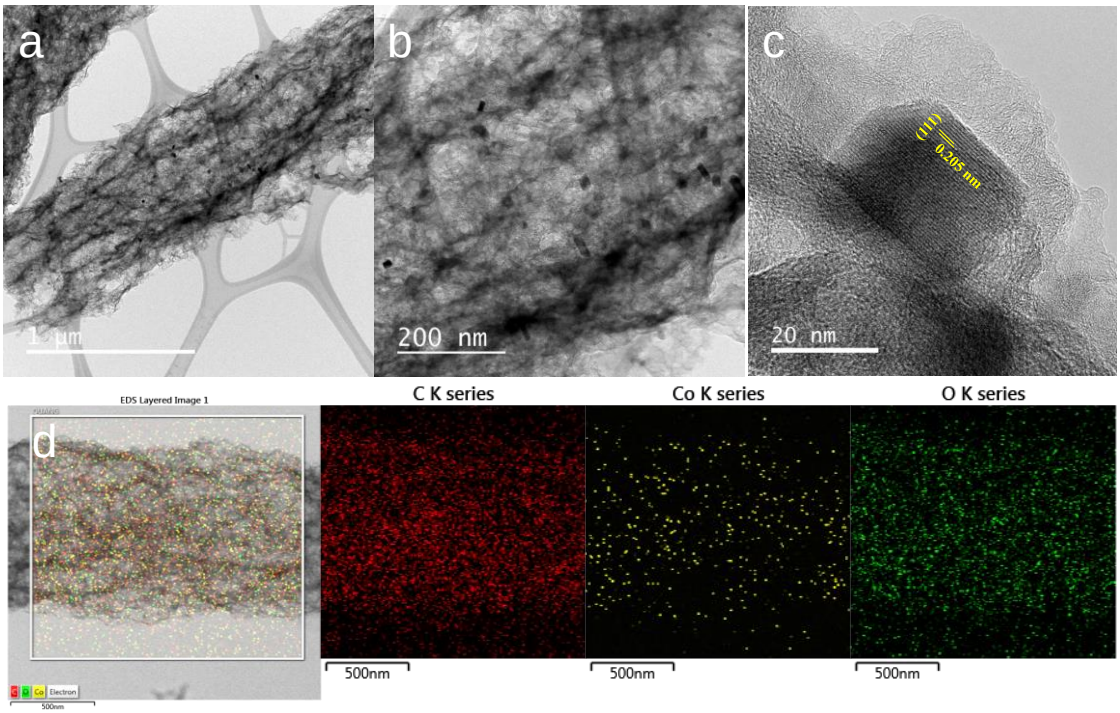

Supplementary Fig. 11 Synthesis and structure characterization of Co-NP/N-SCF catalyst. **a** and **b** HR-TEM image of Co-NP/N-SCF catalyst with different magnification. **c** High magnification HR-TEM image of Co-NP/N-SCF catalyst. **d** Elemental mapping images of Co-NP/N-SCF catalyst.

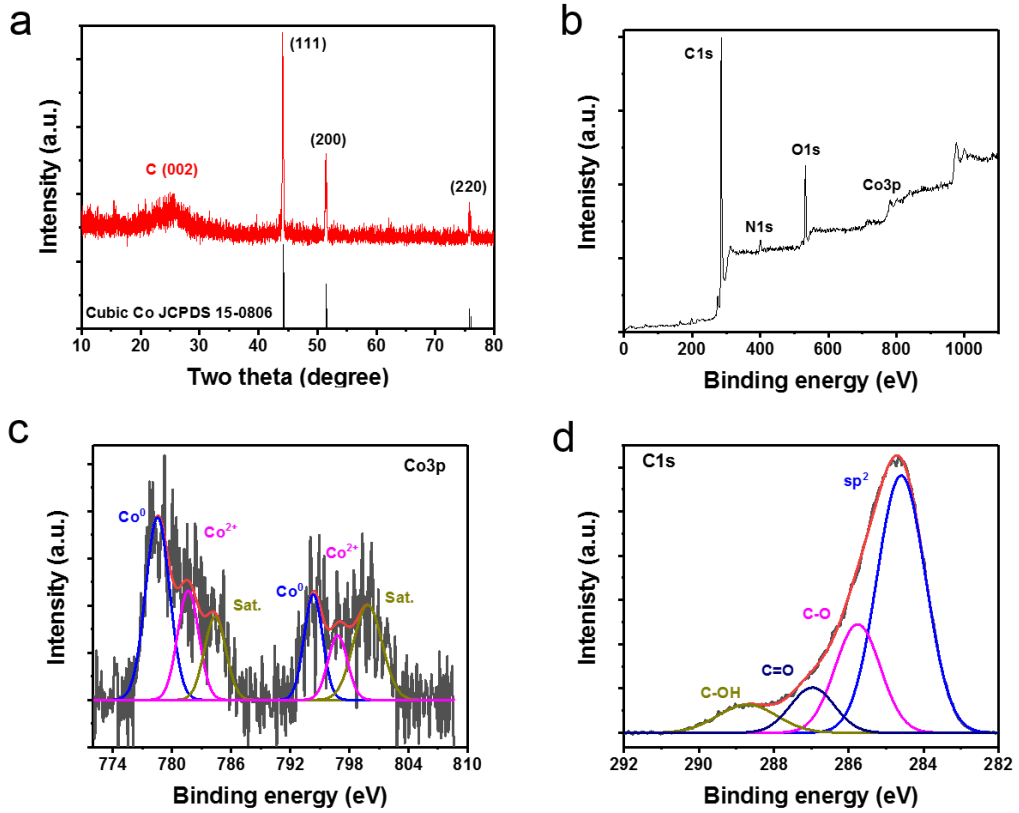

Supplementary Fig. 12 a XRD pattern and **b** XPS spectra for the survey scan of Co-NP/N-SCF catalyst. High-resolution XPS Co *3p* **c** and C *1s* **d** spectra of Co-NP/N-SCF catalyst.

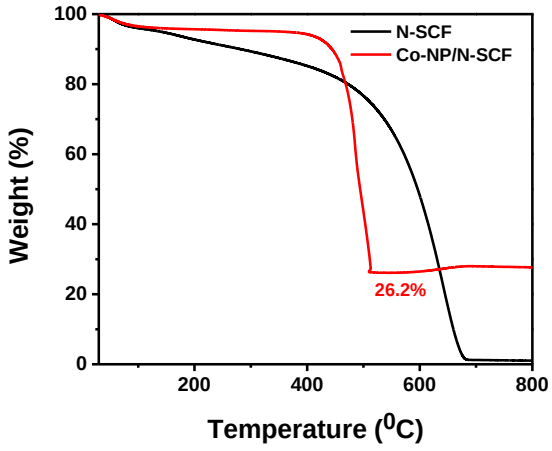

Supplementary Fig. 13 TGA curve of the Co-NP/N-SCF catalyst.

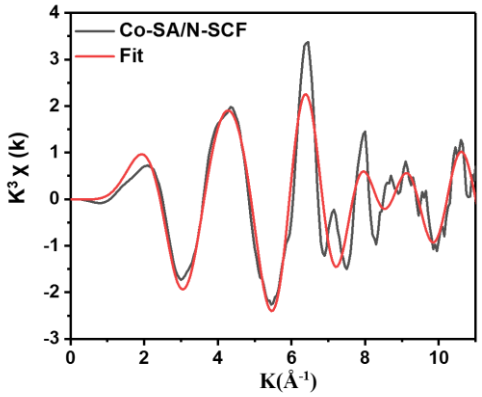

Supplementary Fig. 14 The corresponding EXAFS k space fitting curves of Co-SA/N-SCF.

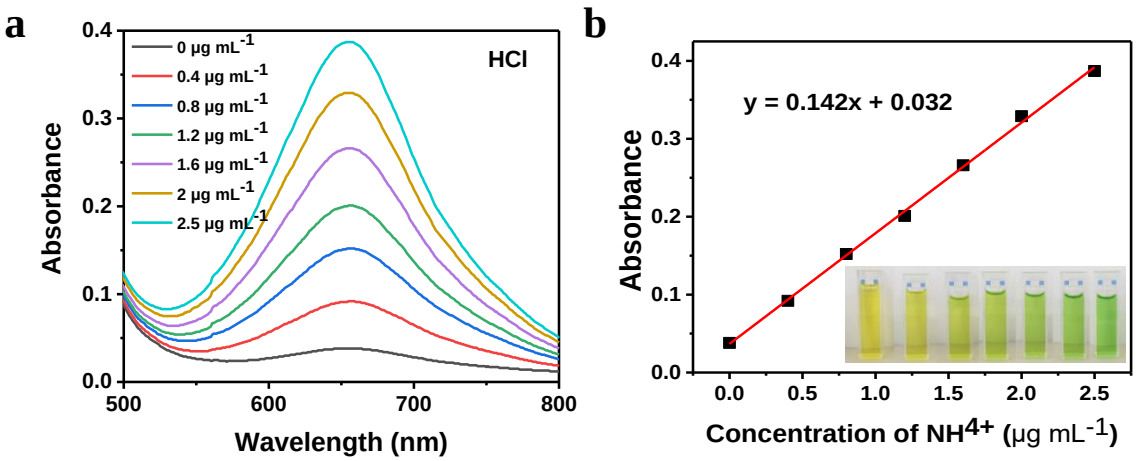

Supplementary Fig. 15 a UV-Vis curves of indophenol blue method and **b** Concentration-absorbance curve of NH_4^+ ions solutions with a species of standard concentration

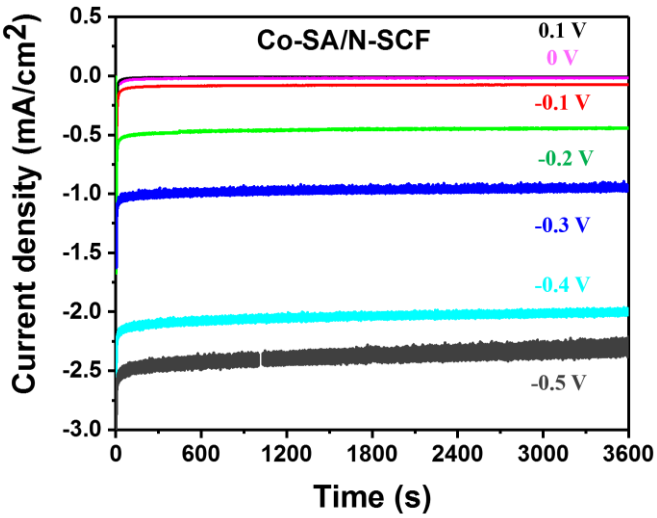

Supplementary Fig. 16 Chronoamperometry results of Co-SA/N-SCF electrode recorded at various applied potentials in N_2-saturated electrolyte for 1h.

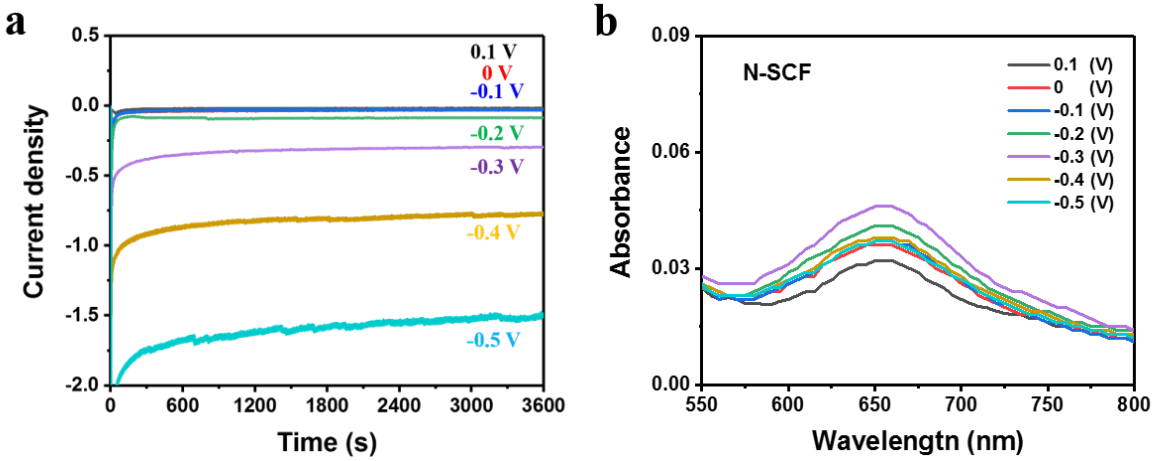

Supplementary Fig. 17 a Chronoamperometry results and **b** UV-vis spectroscopy of the electrolytes stained with an indophenol indicator after NRR electrolysis at various applied potentials in N_2-saturated electrolyte for 1h.

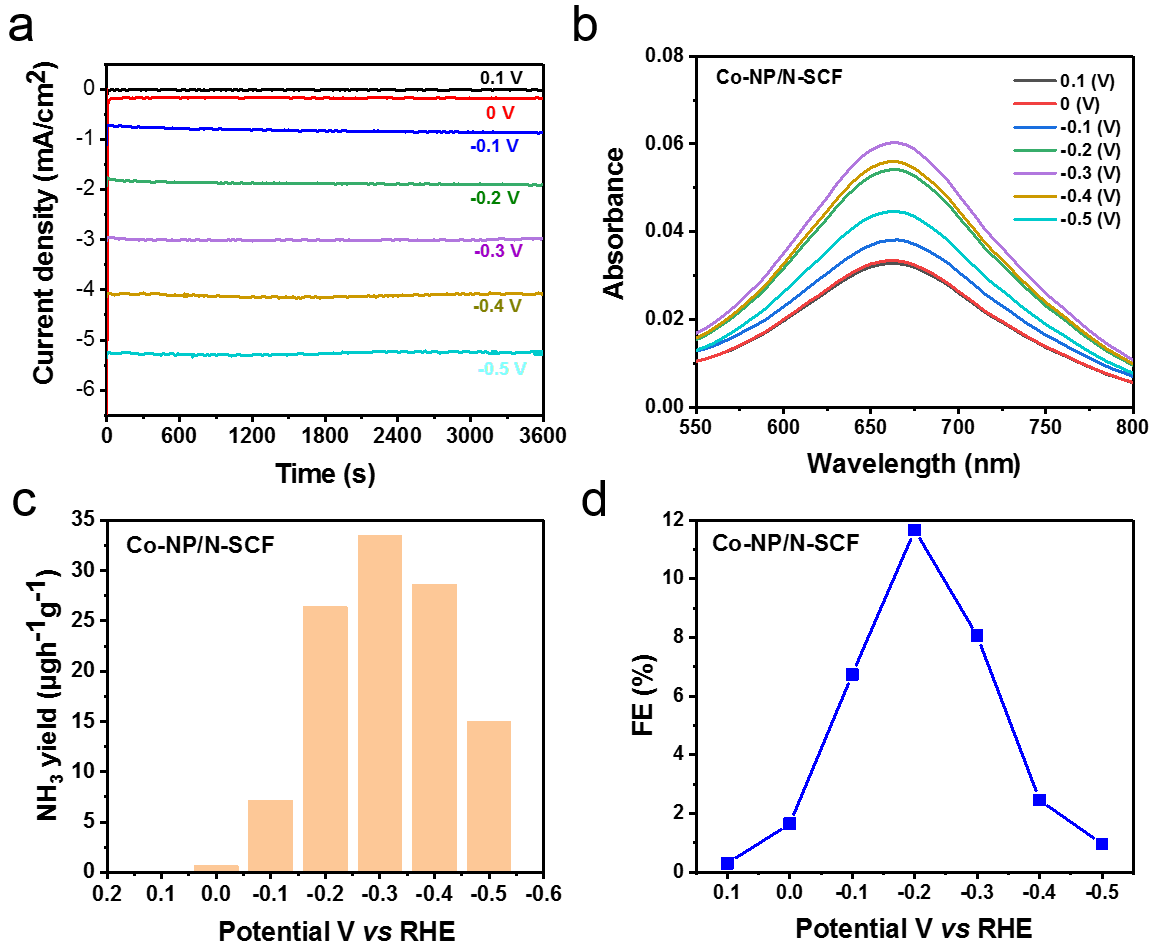

Supplementary Fig. 18 a Chronoamperometry results of Co-NP/N-SCF electrode recorded at various applied potentials in N_2-saturated electrolyte for 1h. **b** UV-vis spectroscopy of the electrolytes stained with an indophenol indicator after NRR electrolysis at various applied potentials in N_2-saturated electrolyte for 1h. **c** NH_3 yield rate and **d** NH_3 Faraday efficiency of Co-NP/N-SCF catalysts at different applied potentials.

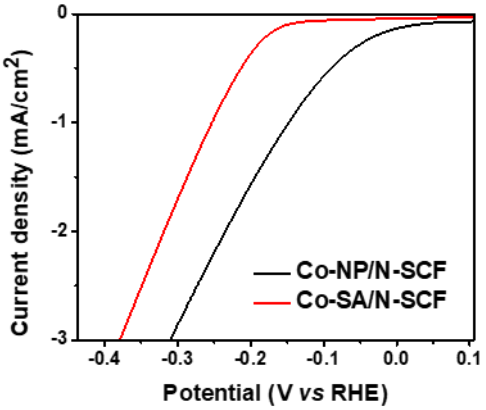

Supplementary Fig. 19 HER activity of Co-SA/N-SCF and Co-NP/N-SCF catalysts.

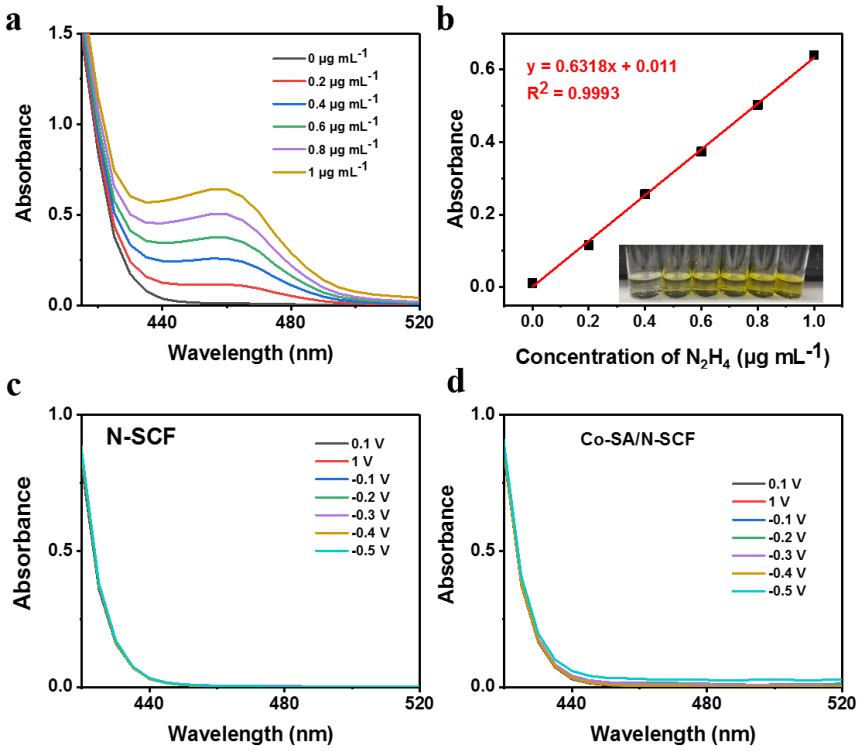

Supplementary Fig. 20 a UV-vis spectroscopy of various $N_2H_4.H_2O$ standard concentration. **b** calibration curve used for the estimation of the $N_2H_4.H_2O$ standard concentration. UV-vis spectroscopy of the electrolytes for N-SCF (**c**) and Co-SA/N-SCF (**d**) after NRR electrolysis at various applied potentials in N_2-saturated electrolyte for 1h.

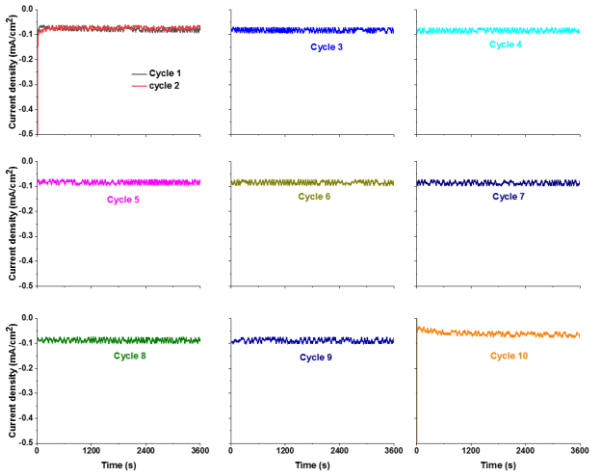

Supplementary Fig. 21 Chronoamperometry results at different NRR cycling stability tests of Co-SA/N-SCF catalyst at -0.1 V *vs* RHE

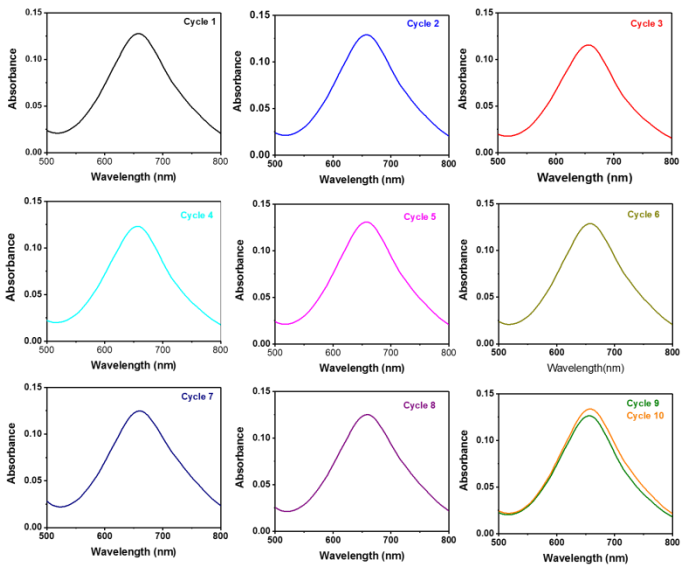

Supplementary Fig. 22 UV-vis spectroscopy of the electrolytes stained with an indophenol indicator at different cycling stability tests of Co-SA/N-SCF catalyst at -0.1 V *vs* RHE

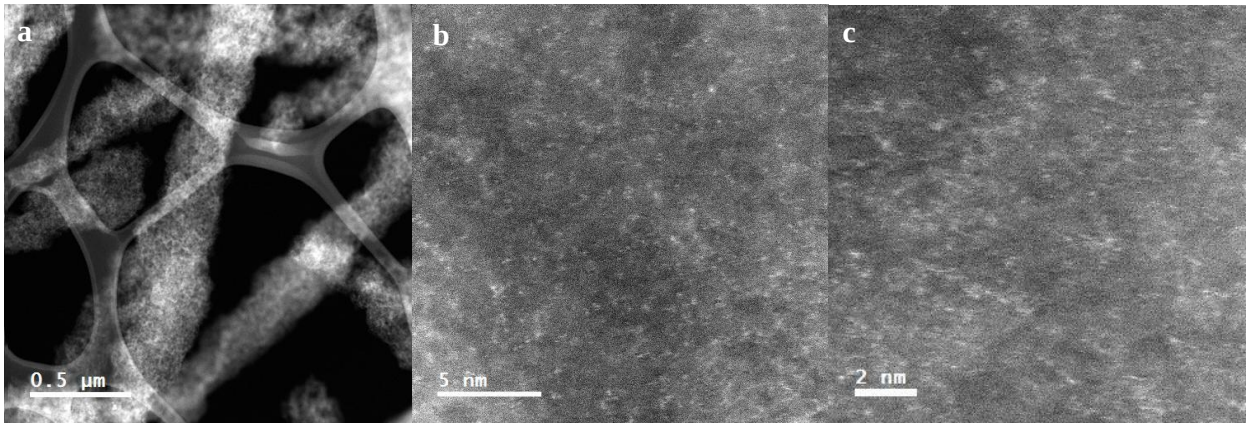

Supplementary Fig. 23 a Low magnification HAADF-STEM image and **b, c** High magnification HAADF-STEM images of Co-SA/N-SCF after cycling stability tests

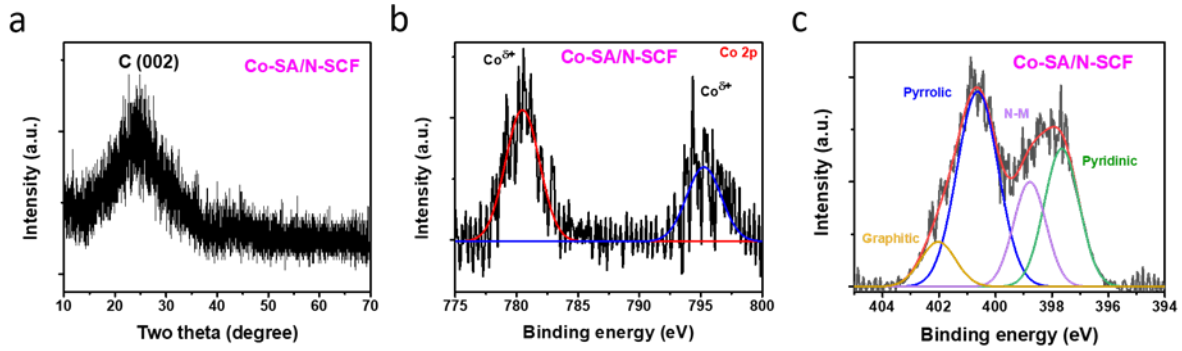

Supplementary Fig. 24 a X-ray diffraction patterns. b High-resolution XPS Co *2p* spectra. c High-resolution XPS N *1s* spectra of Co-SA/N-SCF after cycling stability tests.

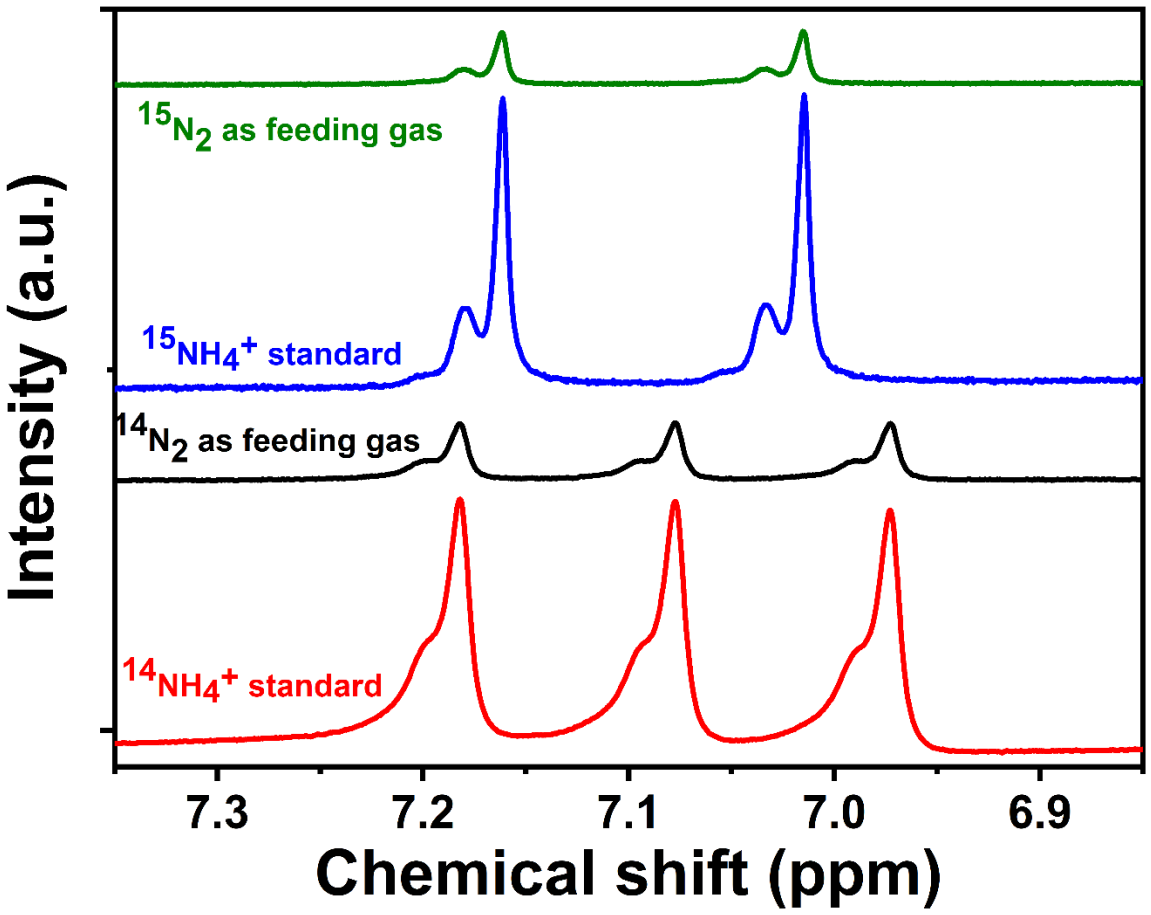

Supplementary Fig. 25 ^{1}H NMR spectra of Co-SA/N-SCF catalyst after electrochemical reduction using $^{15}N_2$- and $^{14}N_2$ as the feed gas together with those of commercial $^{14}NH_4Cl$ and $^{15}NH_4Cl$.

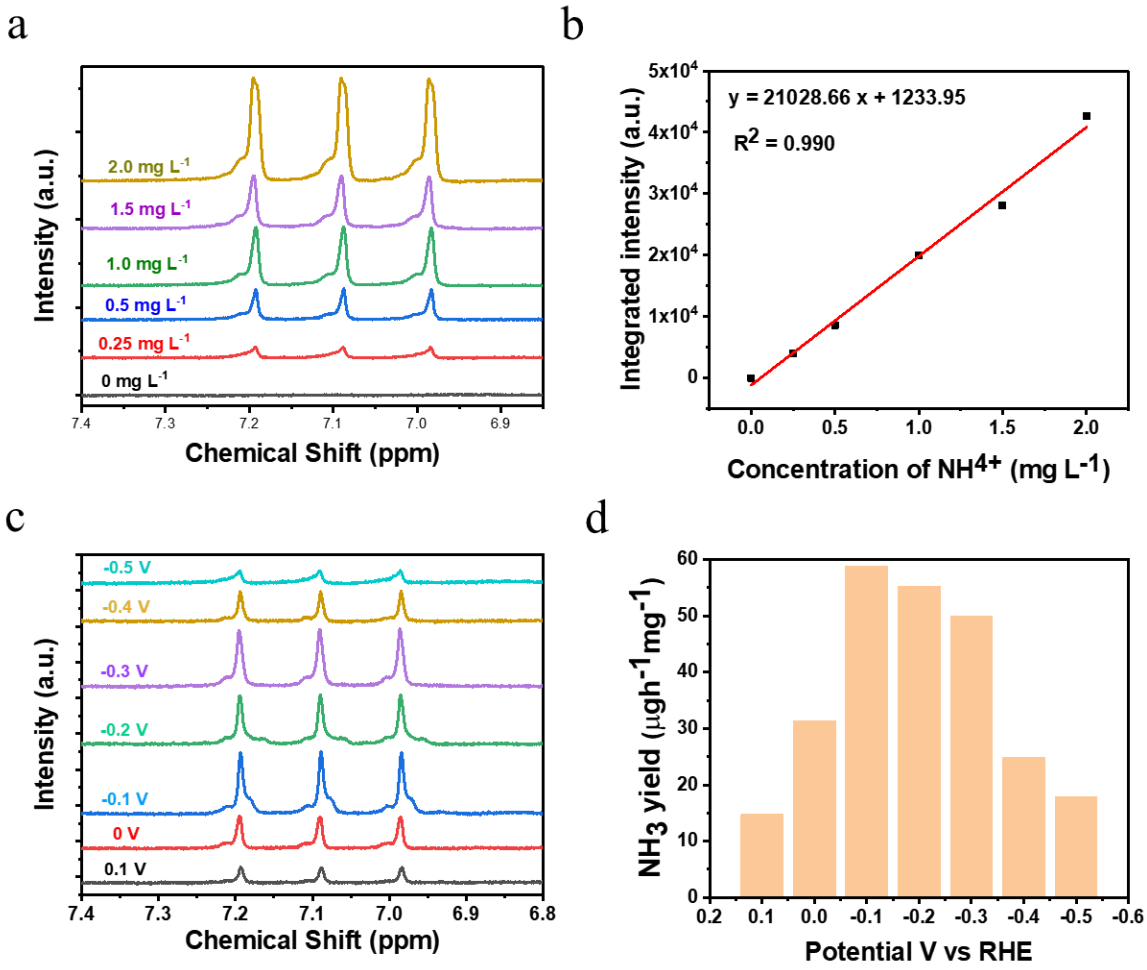

Supplementary Fig. 26 a ^{1}H NMR spectra of the standard solutions with various $^{14}NH_4^+$ concentrations. **b** The corresponding $^{14}NH_4^+$ calibration curve was constructed by plotting the integrated peak areas. **c** ^{1}H NMR spectra of the yielded $^{14}NH_4^+$ by Co-SA/N-SCF electrode in $^{14}N_2$-saturated 0.01 M HCl electrolyte for 1 h period at different potentials. **d** NH_3 yield rates of Co-SA/N-SCF electrode under different applied potentials from ^{1}H NMR method. Note that all the data, including calibration and the products, are calculated by integration area of 7.05-6.95 ppm for quantitatively analyzing the result of NH_4^+ using NMR.

.

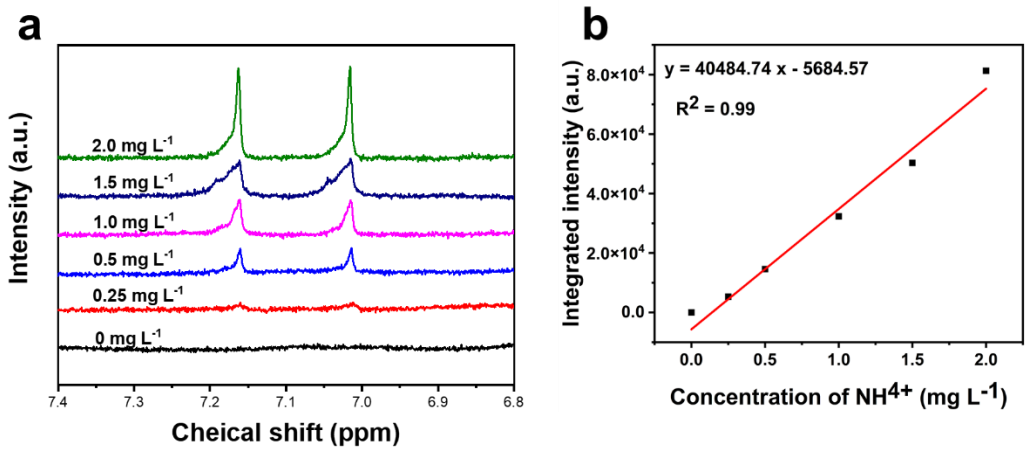

Supplementary Fig. 27 a ^{1}H NMR spectra of the standard solutions with various $^{15}NH_4^+$ concentrations. **b** The corresponding $^{15}NH_4^+$ calibration curve was constructed by plotting the integrated peak areas (6.95~7.10).

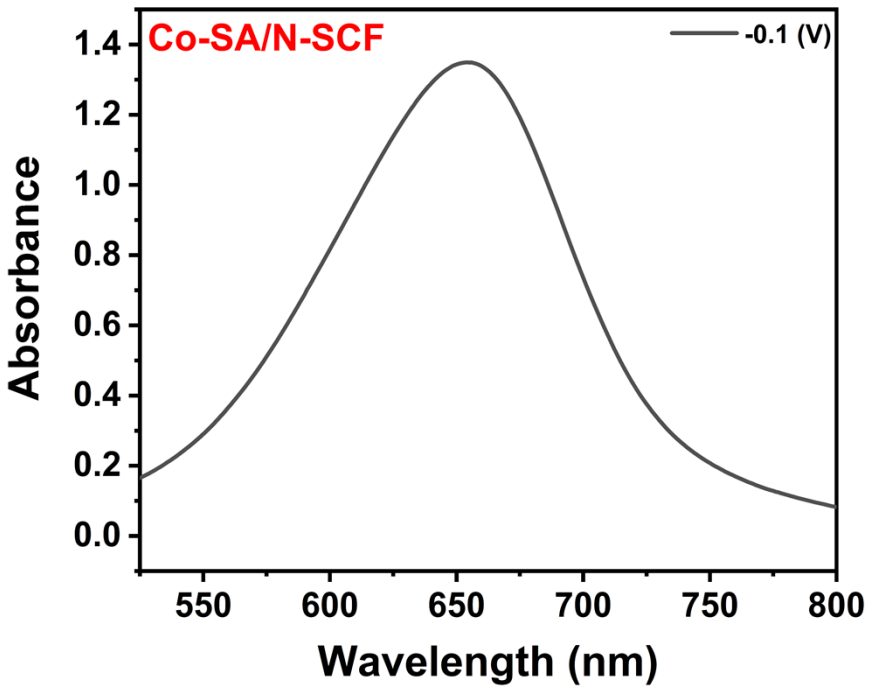

Supplementary Fig. 28 a UV-Vis curves of indophenol at -0.1 V for 12 h using Co-SA/N-SCF catalyst.

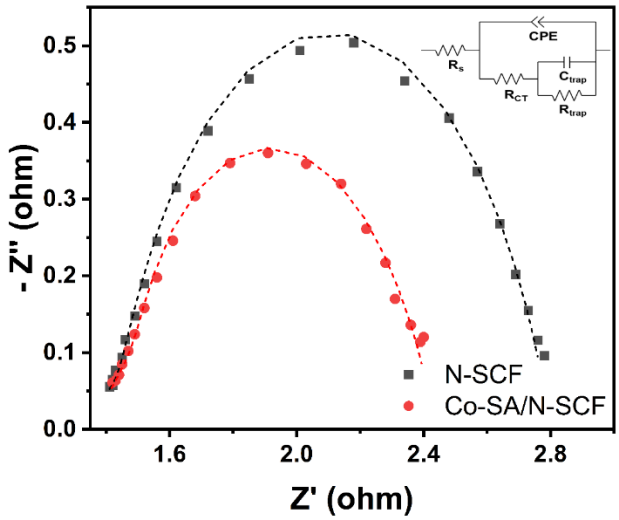

Supplementary Fig. 29 The Nyquist plots of electrochemical impedance spectroscopy (EIS) over N-SCF and Co-SA/N-SCF in 0.01 M HCl.

The table below is the fitting value from the circuit.

	R_s	CPE	R_{CT}	C_{trap}	R_{trap}
N-SCF	1.38E+00	8.36E-04	3.51E-01	6.13E-05	1.06E+01
Co-SA/N-SCF	1.37E+00	1.12E-03	2.91E-01	6.14E-05	7.75E-01

Where Rs is serial resistance; CPE is the constant-phase element; Rct is the charge transfer resistance; Ctrap and Rtrap are related with surface trap resistance.

As a result, we can see that the Co-SA/N-SCF has a small Rct compared to N-SCF, indicating that the less resistance for the charge transfer between the catalyst-electrolyte interface during the NRR reaction.

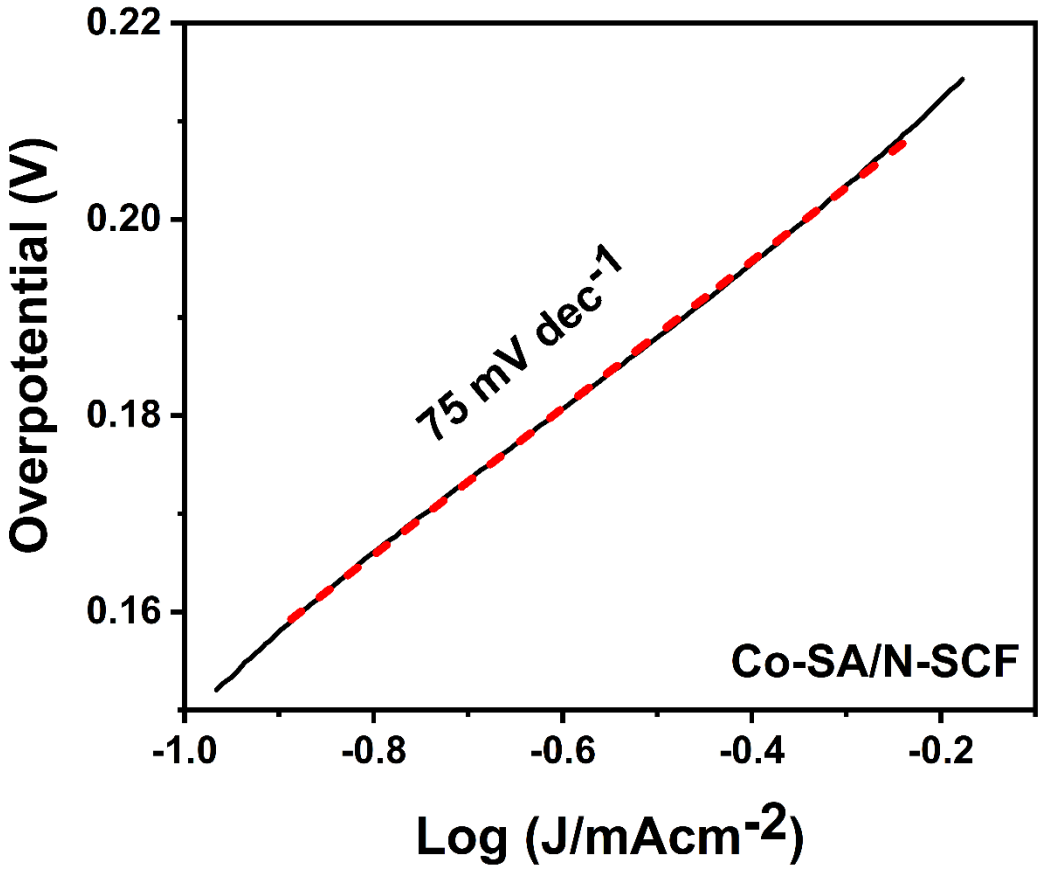

Supplementary Fig. 30 Tafel slope of Co-SA/N-SCF catalyst in 0.01M HCl

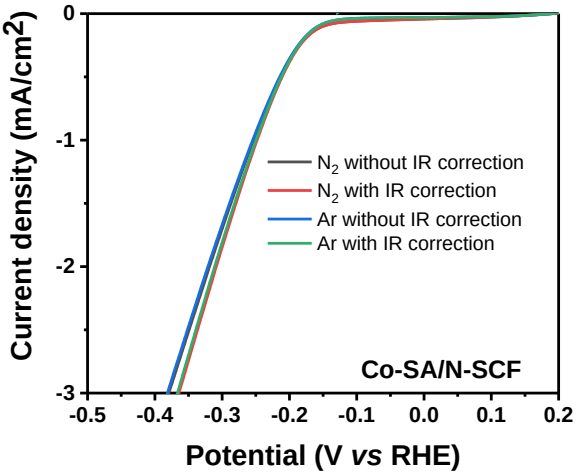

Supplementary Fig. 31 Original and IR-corrected polarization curves of the Co-SA/N-SCF in 0.01 M HCl

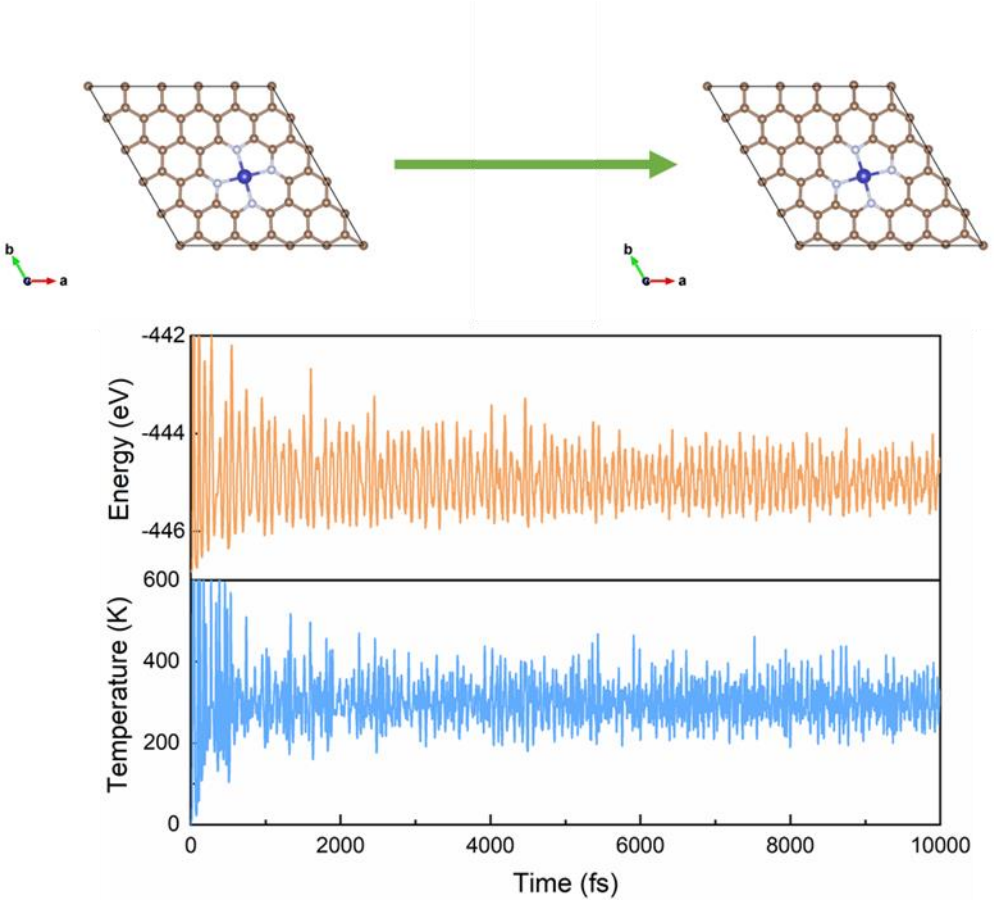

Supplementary Fig. 32 Co-N_4 simulation before and after AIMD at various energies and temperatures.

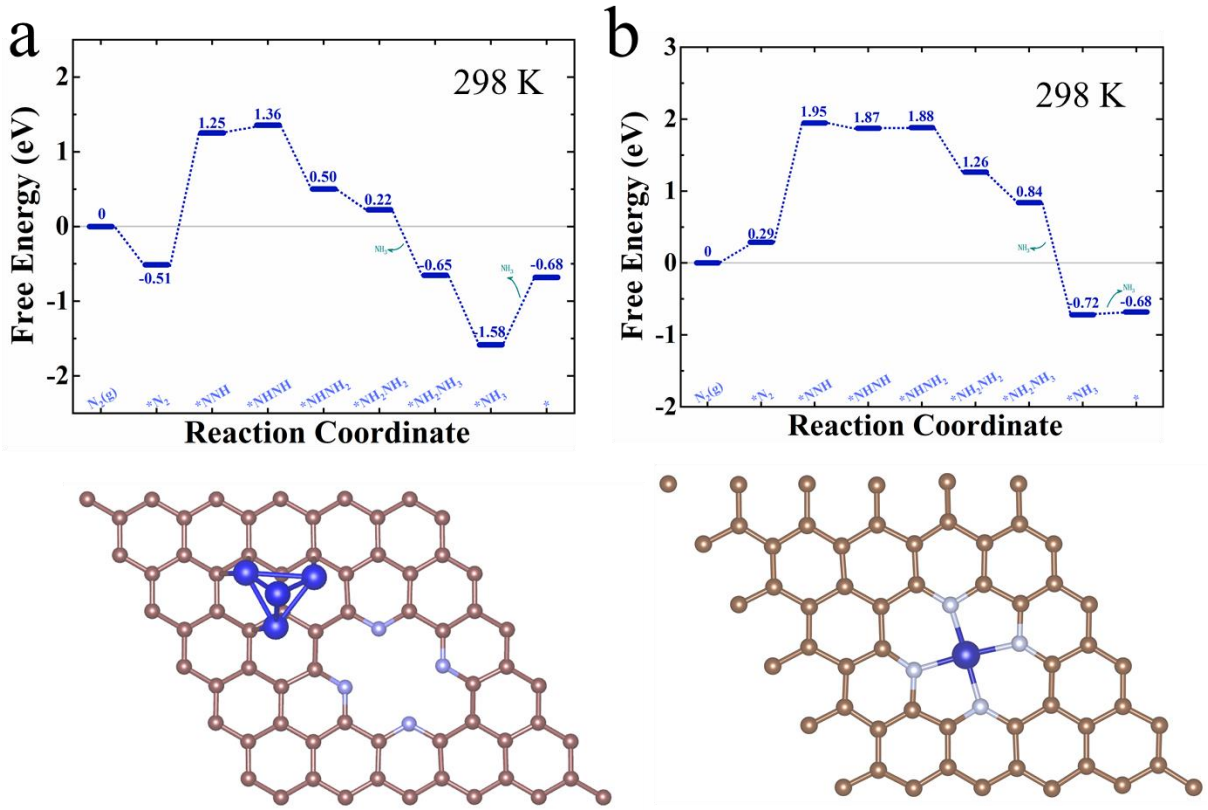

Supplementary Fig. 33 (a) DFT calculation of the possible reaction alternating pathway for electrochemical N_2-to-$2NH_3$ based on the PBE+U for Co-Co bond model at 298 K. (a) DFT calculation of the possible reaction alternating pathway for electrochemical N_2-to-$2NH_3$ based on the PBE+U for Co-N4 model at 298 K.

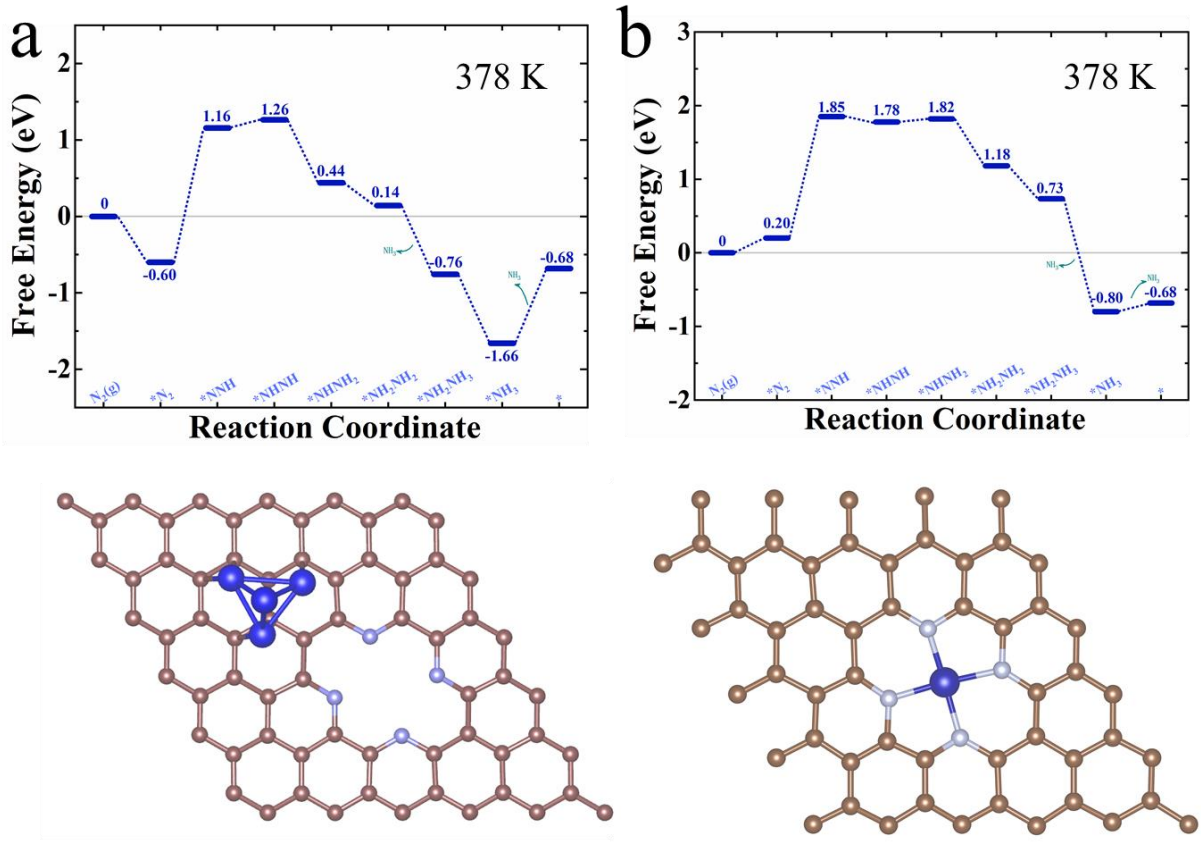

Supplementary Fig. 34 (a) DFT calculation of the possible reaction alternating pathway for electrochemical N_2-to-$2NH_3$ based on the PBE+U for Co-Co bond model at 378 K. (a) DFT calculation of the possible reaction alternating pathway for electrochemical N_2-to-$2NH_3$ based on the PBE+U for Co-N4 model at 378 K.

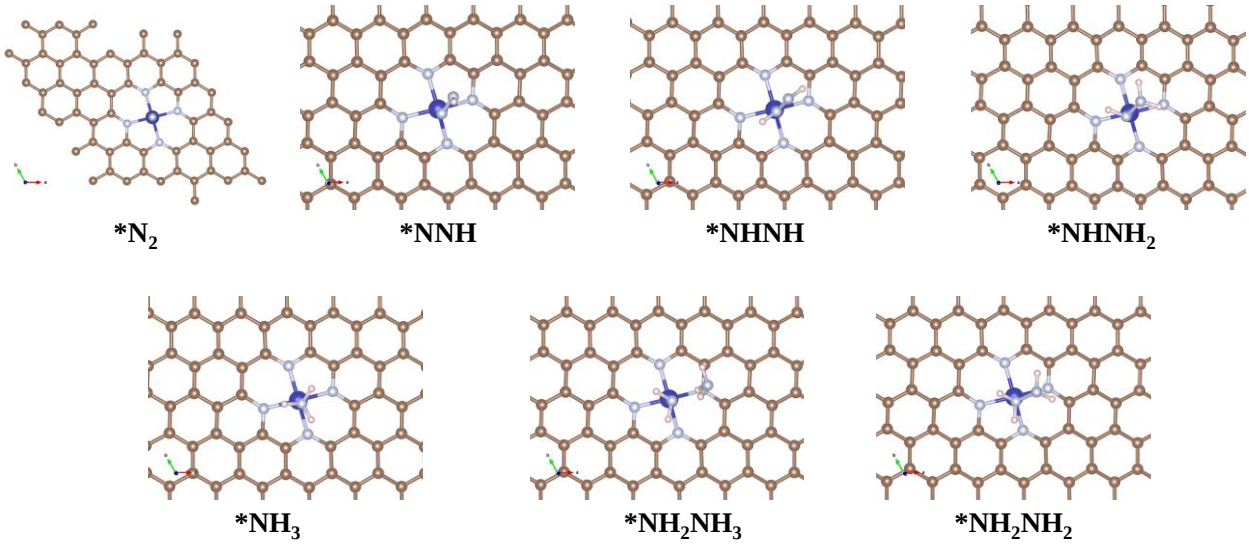

Supplementary Fig. 35 Top-view of the optimized geometric structure of various reaction intermediates along the reaction path of electrochemical N_2-to-NH_3 through alternating mechanisms for Co-N4 bond model.

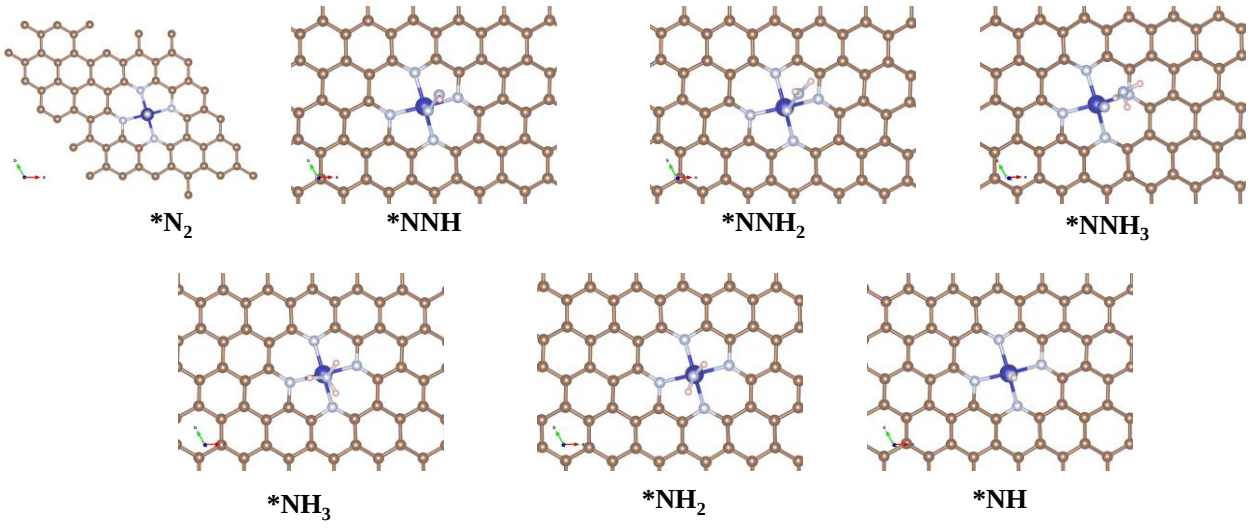

Supplementary Fig. 36 Top-view of the optimized geometric structure of various reaction intermediates along the reaction path of electrochemical N_2-to-NH_3 through distal mechanisms for Co-N4 bond model.

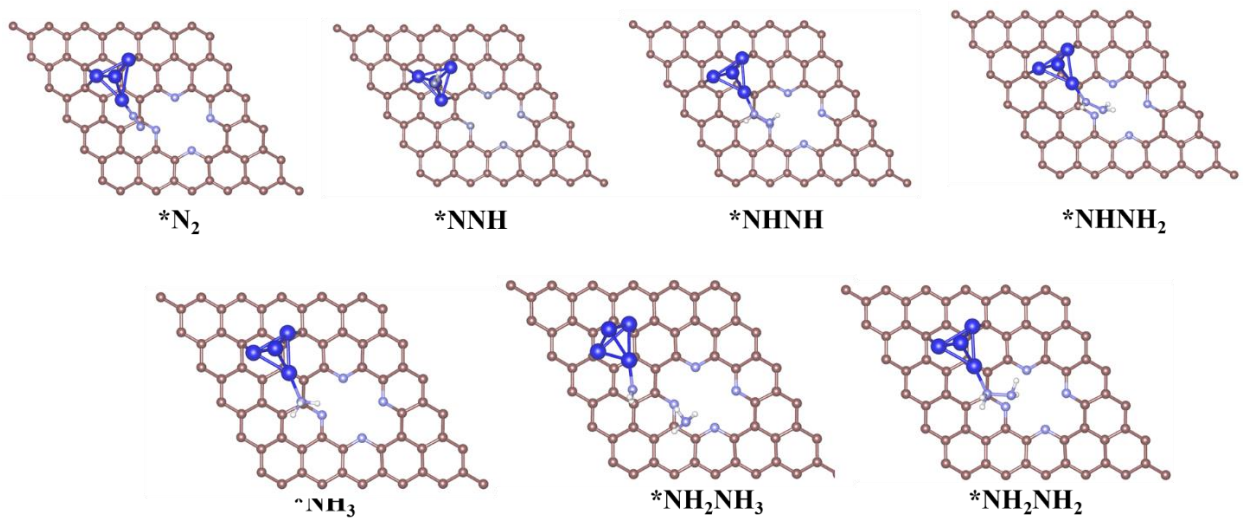

Supplementary Fig. 37 Top-view of the optimized geometric structure of various reaction intermediates along the reaction path of electrochemical N_2-to-NH_3 through alternating mechanisms for Co-Co bond model.

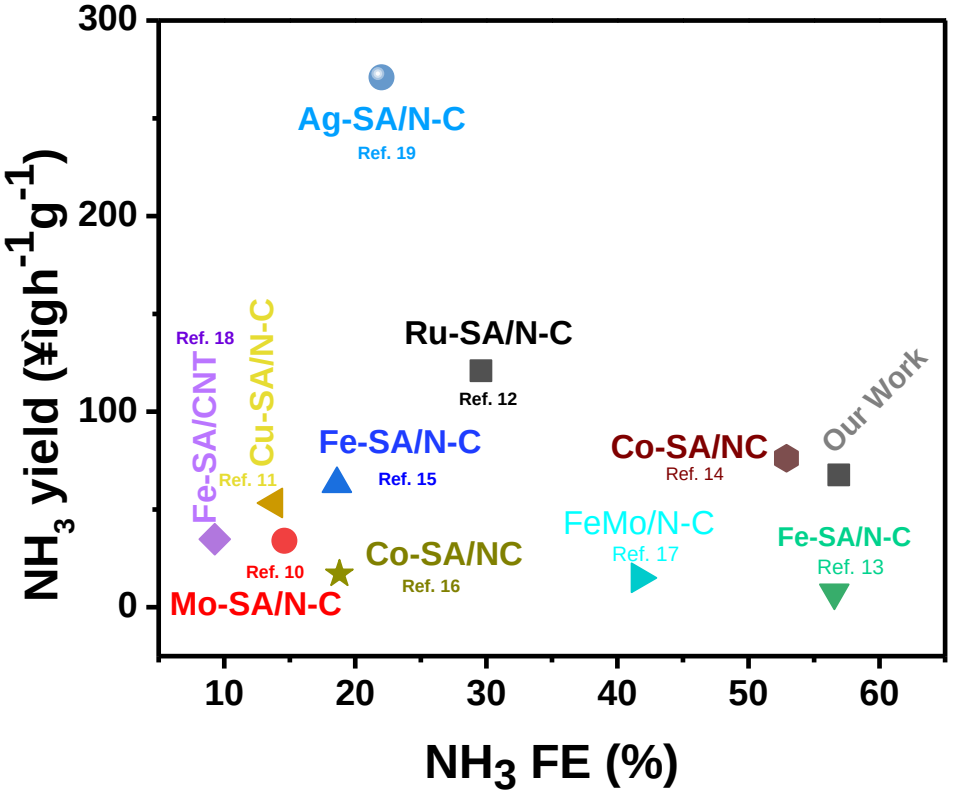

Supplementary Fig. 38 Ammonia yield rate and Faraday efficiency of our catalyst compared with a state-of-the-art single atom-based catalyst[10–19].

Supplementary Table 1: Ammonia yield rate and Faraday efficiency of our catalyst compared with a state-of-the-art single atom-based catalyst.

Catalysts	**Overpotential (V *vs* RHE)**	**NH_3 yield ($\mu g h^{-1} mg^{-1}$)**	**Faraday efficiency (%)**	**References**
Mo-SA/NC	-0.3	34 ± 3.6	14.6 ± 1.6	10
Cu-SA/N-C	-0.35	53.3	13.8	11
Ru-SA/N-C	-0.2	120.9	29.6	12
Fe-SA/NC	0	7.48	56.55	13
Co-SA/NC	-0.2	76.2	52.9	14
Fe-SA/NC	-0.4	62.9 ± 2.7	18.6 ± 0.8	15
Co-SA/NC	-0.25	16.9	18.8	16
FeMo/N-C	-0.2	14.95	41.7	17
Fe-N/C-CNT	-0.2	34.83	9.28	18
Ag-SA/N-C	-0.6	270.9	21.9	19
Co-SAs/N-SCF	-0.1	67.6	56.9	This work

Supplementary Table 2. EXAFS fitting parameters at the Co K-edge.

Sample	Shell	N [a]	R (Å) [b]	σ^2 (Å^2·10^{-3}) [c]	ΔE0 (eV) [d]	*R* factor (%)
Co-SA/N-SCF	Co-N	4.0	1.95	12.3	-6.4	0.3
	Co-Co	0.4	2.51	4.6	-2.8	

[a] *N*: coordination numbers; [b] *R*: bond distance; [c] σ^2: Debye-Waller factors; [d] ΔE_0: the inner potential correction. *R* factor: goodness of fit. *S*02 were set as 0.85/0.9 for Co-N/Co-Co, which were obtained from the experimental EXAFS fit of reference CoPc/Co foil by fixing CN as the known crystallographic value and was fixed to all the samples. Note that a small amount of dimer may exist in the catalyst of Co-SA/N-SCF. But it is not dominant in comparison with single atoms.

Supplementary Table 3. The comparison results of yield of NH_3 using two methods, including the NMR method and Indophenol method.

The potential (vs. RHE)	**0.1 v**	**0 v**	**-0.1 v**	**-0.2 v**	**-0.3 v**	**-0.4 v**	**-0.5 v**
NMR ($ugh^{-1}mg^{-1}$)	14.78	31.5	58.79	55.22	50.03	24.92	17.823
Indophenol method ($ugh^{-1}mg^{-1}$)	14.79	30.98	67.60	59.85	48.59	23.24	19.71

Supplementary Table 4 calculated ZPE and TS value of different species (T=298 K), where the label * denotes the status of adsorption.

Adsorbed species	E_{ZPE} (eV)	TS (eV)
$*N_2$	0.191537	0.187616
* NNH	0.542321	0.162202
* NNH_2	0.852257	0.222358
* NNH_3	1.082374	0.309378
*NH	0.335222	0.159763
*NH_2	0.665784	0.151987
*NH_3	0.996732	0.151000
*NHNH	0.814494	0.182663
*$NHNH_2$	1.133744	0.092769
*NH_2NH_2	1.475881	0.141249
*NH_2NH_3	1.632014	0.178259

Supplementary Table 5 calculated ZPE and TS value of different species (T=378 K), where the label * denotes the status of adsorption.

Adsorbed species	E_{ZPE} (eV)	TS (eV)
$*N_2$	0.191537	0.275427
* NNH	0.542321	0.257406
* NNH_2	0.852257	0.349276
* NNH_3	1.082374	0.470203
*NH	0.335222	0.249338
*NH_2	0.665784	0.237630
*NH_3	0.996732	0.227723
*NHNH	0.814494	0.277496
*$NHNH_2$	1.133744	0.154653
*NH_2NH_2	1.475881	0.222455
*NH_2NH_3	1.632014	0.282395

References

[1] G. Kresse, J. Furthmüller, *Phys. Rev. B* 1996, **54**, 11169.

[2] J. Enkovaara, C. Rostgaard, J. J. Mortensen, J. Chen, M. Dułak, L. Ferrighi, J. Gavnholt, C. Glinsvad, V. Haikola, H. Hansen, *Journal of Physics: Condensed Matter* 2010**, 22**, 253202.

[3] P. E. Blöchl, *Phys. Rev. B* 1994**, 50**, 17953-17979.

[4] G. Kresse, D. Joubert, *Phys. Rev. B* 1999**, 59**, 1758-1775.

[5] J. P. Perdew, K. Burke, M. Ernzerhof, *Phys. Rev. Lett* 1996, **77**, 3865-3868.

[6] V. Singh, M. Kosa, K. Majhi, D. T. Major, *Journal of chemical theory and computation.* 2015**, 11**, 64-72.

[7] M. Cococcioni, S. De Gironcoli, *Phys. Rev. B* 2005**, 71**, 035105.

[8] L. Li, H. Guo, G. Yao, C. Hu, C. Liu, Z. Tian, B. Li, Q. Zhang, L. Chen, *J. Mater. Chem. A* 2020**, 8**, 22327-22334.

[9] J. Zhao, Z. Chen, *J. Am. Chem. Soc.* 2017, **139**, 12480-12487.

[10] L. Han, X. Liu, J. Chen, R. Lin, H. Liu, L. Fang, S. Bak, Z. Liang, S. Zhao, E. Stavitski, J. Luo, R. R. Adzic, H. L. Xin, *Angewandle chemie* 2019, **131**, 2343.

[11] W. Zang, T. Yang, H. Zou, S. Xi, H. Zhang, X. Liu, Z. Kou, Y. Du, Y. P. Feng, L. Shen, L. Duan, J. Wang, S. J. Pennycook, *ACS Catal.* 2019, **9**, 10166.

[12] Z. Geng, Y. Liu, X. Kong, P. Li, K. Li, Z. Liu, J. Du, *Adv. Mater.* 2018, **30**, 1803498.

[13] M. Wang, S. Liu, T. Qian, J. Liu, J. Zhou, J. Zhong, C. Yan, *Nat. Commun.* 2019, **10**, 341.

[14] S. Liu, M. Wang, H. Ji, X. Shen, C. Yan, T. Qian, *Natl. Sci. Rev.* 2020.

[15] F. Lü, S. Zhao, R. Guo, J. He, X. Peng, H. Bao, J. Fu, L. Han, G. Qi, J. Luo, X. Tang, X. Liu, *Nano Energy* 2019, **61**, 420.

[16] S. Zhang, Q. Jiang, T. Shi, Q. Sun, Y. Ye, Y. Lin, L. R. Zheng, *acs Appl. energy Mater.* 2020, **3**, 6079.

[17] Y. Li, Q. Zhang, C. Li, H. Fan, W. Luo, H. Liu, S. Dou, *J. Mater. Chem. A* 2019, **7**, 22242.

[18] Y. Wang, X. Cui, J. Zhao, G. Jia, L. Gu, Q. Zhang, L. Meng, Z. Shi, L. Zheng, C. Wang, Z. Zhang, W. Zheng, *ACS Catal.* 2019, **9**, 336.

[19] Y. Chen, R. Guo, X. Peng, X. Wang, X. Liu, J. Ren, J. He, L. Zhuo, J. Sun, Y. Liu, Y. Wu, J. Luo, *ACS Nano* 2020, **14**, 6938.